ELSEVIER

Nuclear Instruments and Methods in Physics Research B 143 (1998) 441–454

NIM B
Beam Interactions with Materials & Atoms

Angular and impact parameter dependent electron emission in collisions of swift bare and screened heavy ions with gaseous targets

U. Bechthold [a,*], S. Hagmann [b], J. Ullrich [a], B. Bathelt [a], G. Kraft [a], H. Schmidt-Böcking [c]

[a] *Gesellschaft für Schwerionenforschung m.b.H., Biophysik, Planckstraße 1, D-64291 Darmstadt, Germany*
[b] *J.R. Macdonald Laboratory, Kansas State University, Manhattan, Kansas 66506, USA*
[c] *Institut für Kernphysik Uni Frankfurt, August-Euler-Straße 6, D-60486 Frankfurt/Main, Germany*

Received 26 March 1998; received in revised form 2 July 1998

Abstract

We have measured double-differential cross sections of electron production in 3.6 MeV/u neon, xenon and 5.9 MeV/u uranium projectile collisions with gaseous many-electron targets. The paper is focused on the angular dependence of the mean ejected electron energy in the transition from bare (Ne^{10+}) to highly screened (U^{29+}) heavy ions. For some collision systems the electron spectra were measured in coincidence with projectiles that captured an electron from the target. It is well shown in results of presented *n*CTMC-calculations that only small impact parameters contribute to the capture process, thus comparison of coincident and non-coincident spectra reveal the impact parameter dependence of electron emission. © 1998 Elsevier Science B.V. All rights reserved.

Keywords: δ-electron emission; Spectroscopy; Mean ejection energy; Impact parameter dependence; Heavy-ion collision

1. Introduction

In fast ion–atom collisions the projectiles dissipate most of their energy via electronic stopping, i.e., the transfer of kinetic energy into electronic excitation and ionization of the target atoms. About two-thirds of the total energy loss is transformed into kinetic energy of the liberated δ-electrons [1]. In solids, the δ-electrons play the most important role in the formation of particle tracks. This deposition of energy or dose (defined as energy per unit mass) can cause severe damage to sensitive material in, for example, highly integrated circuits in memory chips or CPU's or biological tissue, where damage is expressed in reduced cell survival due to DNA-lesions [2]. Much effort has been put in the understanding of the relationship between energy deposition and final damage. The physical dose deposited in a material is a simple function of the Linear Energy Transfer (LET, equivalent to the energy loss

* Corresponding author.

0168-583X/98/$ – see front matter © 1998 Elsevier Science B.V. All rights reserved.
PII: S0168-583X(98)00415-7

dE/dx in keV/μ) that can be calculated to a high precision using the Bethe–Bloch formula [3]. The response of a biological system on the other hand is extremely sensitive to the local ionization density. Because the ionization density depends on the track diameter as well as on the LET, the velocity v_P, nuclear charge Z_P and charge state q_P of the projectile are crucial parameters. Various models have been developed in order to determine the relative biological efficiency of heavy-ion radiation and explain how ion induced damage is repaired [4]. Application of these models are risk estimation of prolonged space travel in a manned Mars mission and – even more important – heavy-ion radiation cancer therapy [5]. For most of these models it is necessary to have exact electron production cross sections to obtain correct radial dose profiles along the ion tracks [6].

The experiments were performed at energies between 3.6 and 5.9 MeV/u, where projectiles heavier than carbon reach their maximum energy loss per unit length dE/dx in water. Therefore we are sensitive on the energy that a projectile has at the last few μm of its path, before it is completely stopped in the target. At these energies, the energy loss per unit length reaches its maximum in the so-called 'Bragg-peak', that is close to the maximum of the relative biological efficiency of heavy-ion radiation.

Because the energy spectra of the emitted electrons are of great importance for the formation of damage, we will discuss in detail the features, that can be observed in ejected electron spectra after ion–atom collisions. First, there is an exponentially decreasing background of the so-called Three-Body-Encounter (TBE) [7] electrons, emitted in soft, distant collisions. These electrons are scattered by the potentials of the projectile and the target core, resulting in a nearly isotropic angular distribution. In general, this is the process with the largest production cross section over the complete electron energy interval.

Second, Auger electrons from inner shell ionization or double excitation are observed as distinct peaks superimposed on the background by TBE electrons. The analysis of their energy, angular distribution and production cross section dependence from the projectile energy reveals a wealth of information about target species and charge state, ionization dynamics and basic resonant ion–atom interactions [8]. Nevertheless, the contribution of Auger electrons to the total ionization cross section is negligible in most cases.

If the projectile is carrying loosely bound electrons, the cusp shaped peak from Electron-Loss-to-the-Continuum (ELC) [9] is visible at an electron energy that corresponds to the projectile velocity v_P. This process is regarded as low energy electron emission in the moving projectile reference frame. Furthermore, target Electron-Capture-to-the-Continuum (ECC) [10] states of the projectile is another process that leads to an emission at v_P. Because of kinematic reasons, ECC emission is strongly peaked around 0°.

The next contribution are electrons generated in hard, close collisions between the ion and the target atom. Because their energy distribution essentially depends on only two collision partners they are called 'Binary Encounter' electrons (BEe) [11]. The energy of BEe strongly depends on the laboratory observation angle according to

$$E_e = 4\frac{m_e}{M_P}E_P\cos^2(\vartheta_e), \tag{1}$$

with m_e being the electron mass, M_P, E_P being projectile mass and energy and ϑ_e the electron ejection angle in the laboratory system. Within the Impulse Approximation (IA) [12] the Binary Encounter emission is treated as Rutherford scattering of a quasi-free target electron in the projectile rest frame. Due to the initial momentum distribution of the target electron (Compton-profile) the binary emission finally appears as a very broad peak having a Gaussian shape. According to Eq. (1) the BEe energy decreases towards larger laboratory angles, while the cross section increases. At forward angles the Binary Encounter process leads to the electron emission with the highest observable energy, therefore the range of the BEe in a solid is generally used as the track radius. At angles larger than about 60° the BE peak is hardly discernible from the TBE electrons.

The contributions from TBE, ECC, ELC and BE are generally summarized as δ-electrons. In collisions with bare, light projectiles, the variation in the electron production cross section from zero

energy to beyond the Binary Encounter peak is usually in the order of more than four orders of magnitude. However, in collisions with light and bare ions, the major part of projectile energy loss is deposited in electrons with energies smaller than 500 eV, thus leading to a mean electron energy $\langle E_e \rangle$ of a few 100 eV [13].

Electron spectra, doubly differential in energy and laboratory emission angle ϑ_e have been measured to a large extent for light ions (p, He) with energies in the 100 keV/u to a few 10 MeV/u regime [14]. Targets commonly used were rare gases and few atom molecular gases like H_2, H_2O, N_2, O_2 and carbohydrates [15]. In these experiments the data fit well to predictions of first order theories (First Born Approximation, Binary Encounter Approximation) where the cross sections scale with $(q_P/E_P)^2$, with q_P as the ionic charge, and with the number of 'active' target electrons, i.e. electrons with an orbital velocity smaller than the projectile velocity. Later, these findings were extended to heavier projectiles like bare neon and argon [16]. In the mid 1980s Kelbch and Schmidt found surprising structures in electron spectra for 1.4 MeV/u U^{33+} ions [17]. The scaling laws found for bare ions were not applicable in these experiments. The unexpected features encountered in these spectra included a sudden energy shift of the BE peak within a narrow angular interval, and a splitting of the peak into two components. In addition it was found, that in experiments with fast, very heavy projectiles with low charge states the emission of high energy Binary Encounter electrons in forward direction is dramatically enhanced. It was subsequently demonstrated, that the origin of all these new findings is based in the non-Coulomb nature of the screened field of the projectile [18–21]. It is responsible for both the zero-degree enhancement of the cross section and the appearance of diffraction minima and maxima for elastic scattering of electrons in the projectile field. The diffraction effects, i.e. the interference of partial waves of the incoming electron, give rise to the observed non-classical behavior of the BE peak, and qualitatively reproduce the experimental results [22,23]. Furthermore, it should be noted that the effects caused by screening of the nuclear potential are strongly dependent on q_P, Z_P and E_P, with a maximum towards high Z_P, low q_P and energies in the 0.5–5 MeV/u regime [19].

For applications in condensed phase the electron production cross sections of gas targets are scaled by the target density to model situations, where ions penetrate solid state or liquid targets [24]. This procedure is problematic, because many of the collective effects in dense material like phonon and plasmon excitation, etc. are completely neglected. In gas targets all impact parameters b between 0 and ∞ are possible, whereas in solids b is limited to zero and about half the lattice constant. In order to quantitatively understand the process of electron liberation in solids it is desirable to have targets of mono-layer thickness to fulfill the single collision condition. (However, mono-layer targets could not model the situation in a bulk material, since the electronic structure concerning plasmon excitation, dielectric function, etc. of very thin layers is quite different to extended solids.) In practice, it is not possible to manufacture self-supporting foils of mono-layer thickness. Using thicker foils, the electrons will undergo subsequent collisions, and complex transport phenomena have to be included for the interpretation of the spectra; the initial information about the single collision is lost. In our experiments we want to simulate the solid state conditions in a single collision by a selection of only those electrons that are liberated in collisions with small impact parameters in ion–gas collisions. Thus, surface effects and surface electronic states that usually come into play can be ruled out. It is achieved by coincidental measurement of projectile electron capture and simultaneous target ionization. Of course, this procedure will not be able to yield any information about the collective effects in a solid.

2. Experimental setup and conditions

In order to enhance the detection efficiency over former designs, a toroidal electron energy analyzer was developed by one of the authors (S.H.). In contrast to the design of conventional spherical analyzers, the toroid's curvature radius in the dispersive direction does not correspond to a

point, but to a circle, as shown in Fig. 1. Thus, it is possible to obtain a field free target area inside a large gas cell and, for example, integrate foil target holders or a time-of-flight recoil ion spectrometer for coincidence experiments, if desired.

The projectile ion beam was produced in the ECR source at GSI Darmstadt and accelerated to 3.6 (Ne^{10+}, Xe^{40+}) and 5.9 MeV/u (U^{29+}) by the UNILAC. The well collimated ion beam enters the spectrometer through a 10 mm drilling in the outer negative electrode, interacts with the gas target effusing through a 0.7 mm hypodermic needle 4 mm above the beam axis and leaves through another 10 mm drilling. The ion beam is collected in a shielded Faraday cup for normalization to the number of projectiles. The emitted electrons are energy analyzed in the electrostatic field between the two toroidal electrodes. After passing a 3 mm aperture at the exit of the analyzing field, an Einzel lens is being used for transport of the diverging trajectories onto a micro channel plate (MCP) detector. After amplification by the MCP's, a wedge and strip anode is employed for two-dimensional readout of the position information. A high transmission mesh at the potential of -10 V prevents low energy electrons from entering the MCP. A subsequent potential of +200 V accelerates the electrons onto the MCP's for better detection efficiency. The laboratory emission angle is obtained from the position of the electron for each event on the MCP relative to the direction of the beam axis on the focal ring. The simultaneously observable angular range is therefore from 0° to 180° on both sides of the beam axis. Due to the extended source volume, the angular resolution is about 4° in forward direction and 16° perpendicular to the beam axis. The voltage on the toroidal plates is scanned between 0 and $\pm$4000 V, emission energies between 0 and 20000 eV are accessible. The energy resolution was set through entrance slits in the gas cell to 8% for the neon and xenon experiments and to 4% for the uranium projectile. The spectrometer is magnetically shielded by two layers of mu-metal, and reliable data are available for energies down to 20 eV. The spectrometer chamber was pumped to 4×10^{-7} mbar during the experiments. Target pressures were in the order of 10^{-4}–10^{-5} mbar, thus estab-

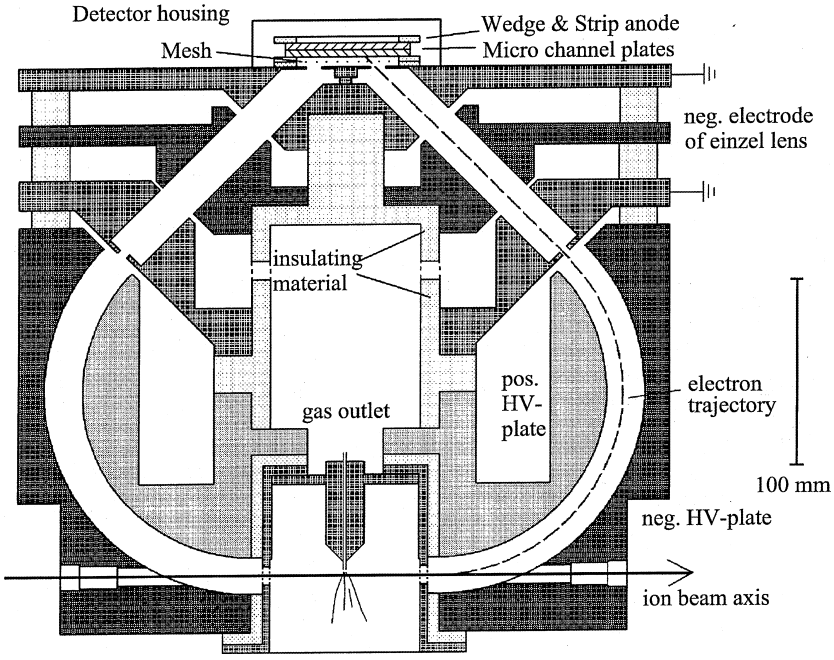

Fig. 1. Sketch of the used toroidal electron analyzer. The apparatus is rotationally symmetric around the axis in the center.

lishing single collision conditions. Background electrons produced by scattering of ions on the metal surfaces of collimation slits and spectrometer parts were carefully reduced and measured without target gas for later subtraction. The charge state was analyzed by a 22.5° magnet about 1500 mm downstream of the reaction zone in the spectrometer. A scintillation detector 2915 mm (Ne^{9+}) resp. 4565 mm (Xe^{39+}) away from the spectrometer center was used to detect the projectiles that captured an electron, while the ion beam with the original charge state was collected in a Faraday cup. A Time-to-Amplitude-Converter (TAC) was started by an electron signal (low count rate) and stopped by the next projectile signal, that was delayed by 126 ns. The conversion time window of the TAC was set to 500 ns. Considering the time-of-flight of the neon projectiles of 111 ns (xenon 174 ns) from the spectrometer to the detector and the time of flight of the electrons it was ensured that all electrons between 10 eV and 12 keV were able to trigger a coincidence event.

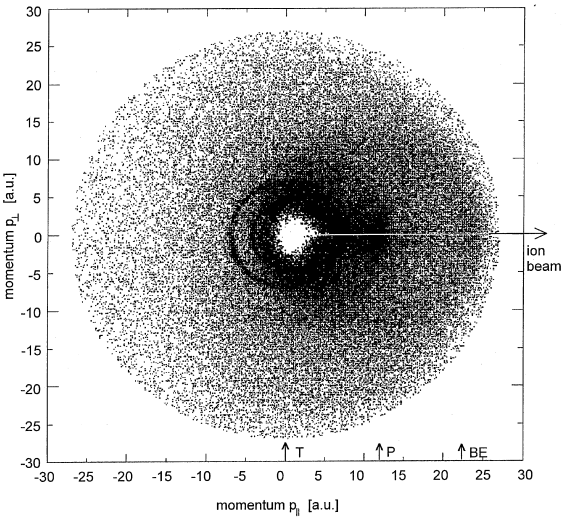

Fig. 2. Complete two-dimensional final state momentum space for electrons emitted in collisions of 3.59 MeV/u Ne^{10+} with C_2F_6.

3. Results and discussion

3.1. Doubly differential electron spectra in collisions of heavy ions with many-electron targets

The spectrometer allows a 360° view of the final state electron momentum space of the collision system, as shown in Fig. 2 for a bare 3.6 MeV/u Ne^{10+} on hexafluorethane C_2F_6.

The components parallel to the beam direction (0°) are plotted on the x-axis, and perpendicular on the y-axis resp., both in atomic units (a.u.) of momentum. For better clarity of the reaction kinematics we use momentum space in this representation, otherwise energy will be given in eV. The density of the points is proportional to $\log_{10}(d^2\sigma/d\Omega dv)$. The values are cut off for a large number of counts, for improved visibility of low intensity structures, being responsible for the white space around (0,0).

The center of the laboratory reference frame is at (0,0), where the maximum of the emission of the so-called TBE-electrons is located. These electrons are due to glancing collisions between the projectile and the target. The emission takes place in the potentials of both the target core and the projectile, which are treated to be of comparable strength. The emission is slightly focused to the forward direction, as a result of the projectile electron interaction after the collision. The circular structures around (0,0) with radii of 4 and 7.5 a.u. in the backward hemisphere are due to KLL-Auger electrons of the carbon and fluorine atoms in the C_2F_6 molecule. In the forward hemisphere they are not discernible from the superimposed background of δ-electrons. At (12,0), the projectile velocity v_P, a peak due to Electron-Capture-to-the-Continuum states appears and is strongly peaked in forward direction. It is the center of the projectile reference frame. The emission of BEe originating from hard projectile–target collisions is a broad ridge with a radius of 12 a.u. around the center of the projectile reference frame at (12,0). It is obvious, that Binary Encounter emission might be regarded as elastic scattering of a target electron with $-v_P$ in the projectile potential in a projectile centered reference frame. In this reference frame, electrons 'start' at (24,0) and travel at v_P to (12,0). Most electrons are not scattered and are left at rest in the target frame. If the impact parameter is small enough and momentum transfer is large, the

electrons are scattered at an angle θ_e in the projectile frame. In a knock-on collision finally, the electrons are scattered by backwards with v_P. In the lab frame it is identical with an acceleration to $2v_P$ at 0°. According to the Rutherford scattering formula for Coulomb potentials the angular dependence of the scattering cross section is proportional to $1/\sin^4(\theta_e/2)$ in the projectile frame.

For all angles from 0° to 180° (in steps of 10°) spectra, doubly differential in energy and ejection angle, have been extracted from momentum spectra for all measured collision systems. Ne, H_2O, C_2H_5OH, Xe, C_2F_6, C_3F_8 and SF_6 were used as target gases. The mean energies have been calculated using the following formula:

$$\langle E(\vartheta)\rangle = \frac{\int_{10}^{E\,\max} N(E,\vartheta) \ * \ E\,\mathrm{dE}}{\int_{10}^{E\,\max} N(E,\vartheta)\,\mathrm{d}E} \qquad (2)$$

Data below 10 eV were not used, due to large uncertainties in the detection efficiency and, primarily, due to the influence of the residual magnetic field of about 10 mG. This results in mean energies that are slightly too high, but the systematic error is not expected to be larger than 10–15%.

3.2. Mean ejected electron energies in collisions with 3.6 MeV/u Ne^{10+}

The left scale of Fig. 3 shows the mean energy of electron emission in the 3.6 MeV/u Ne^{10+} on C_2F_6 collision system.

The mean energy is highest (550 eV) at 0° and decreases exponentially to large angles until it is about 200 eV at 180°. The maximum of the mean energy at forward angles has two reasons: first, there is the contribution of high energy electrons caused by binary collisions and ELC processes. However, the number of electrons from these processes is rather small compared to the total number of electrons emitted in bare ion atom collisions. Second, and more important, there is a significant shift of the angular distribution of low energy electrons toward 0°, as seen as the asymmetric white space around the origin in Fig. 2. The strong long ranging post collision interaction between the highly charged Ne^{10+}-ion and the outgoing electrons leads to a focusing and acceleration towards the projectile.

The cross section of Binary Encounter production in collisions with bare ions can be determined by evaluation of the Rutherford

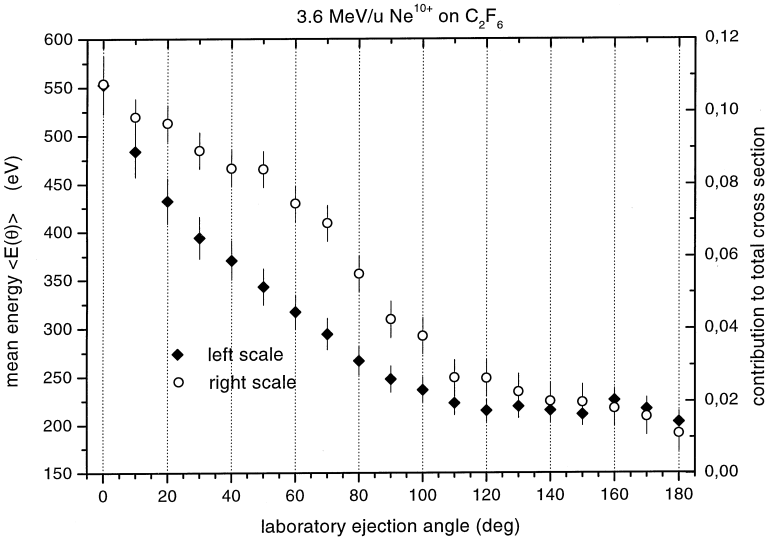

Fig. 3. Right scale: Contribution of a section 10° wide at angle ϑ to the total emission in collisions of 3.6 MeV/u Ne^{10+} with C_2F_6. Left scale: Mean electron emission energies.

scattering model in the projectile rest frame [33]. The Binary emission vanishes at 90° and because there are no other electron emissions other than TBE- and Auger electrons at angles between 100° and 180° the variation of $\langle E(\vartheta)\rangle$ is small.

On the right scale of the figure the contribution of each angular section to the total emission is displayed. The contribution of a 10° segment in forward direction to the complete emission is about 11% and decreases to 1.3% for the backward direction. About 29% of the total electron emission is directed into a cone with 50° opening angle around 0°. The weighted mean energy is about 360 eV for the emission at all angles. This value is higher than the mean electron energy obtained in experiments for example with a proton beam of comparable impact energy. It is expected that this as well is due to the strong post collision projectile–electron interaction (PCI) of the long ranging Coulomb force, which focuses the emitted electron towards the ion.

3.3. Mean ejected electron energies in collisions with 3.6 MeV/u Xe^{40+}

In Fig. 4 the mean ejected electron energies are plotted for the equal velocity 3.6 MeV/u Xe^{40+} on SF_6. In this projectile the nuclear potential is screened by 14 electrons.

The mean energy for 0° is about 800 eV and decreases to 300 eV in backward direction. Again, the attractive force between the highly charged xenon projectile and the emitted electrons leads to a focusing towards the ion direction that is even stronger than in the neon collision, resulting in the observed increase of the mean energy.

Furthermore, it has already been described in literature [19,25], that the screening of the projectile leads to an enhancement of the BE cross section over the one classically scaled with the square of the ionic charge (q_P^2). Compared to the classical Rutherford cross section the surplus of fast electrons at 0° is about a factor of 3 [26] in this collision. The enhancement over Rutherford cross sections affects mainly the emission of BE electrons at laboratory angles up to 30°. This increases the mean energy of the ejected electrons, and is reflected in the contribution of each angular section to the total emission. At 0° it is 17.5% decreasing to 1% for 180°. Almost 44% of the total number of electrons are emitted into a cone with 50° opening angle centered around the beam direction. The weighted mean energy for the overall electron emission increases to about 510 eV.

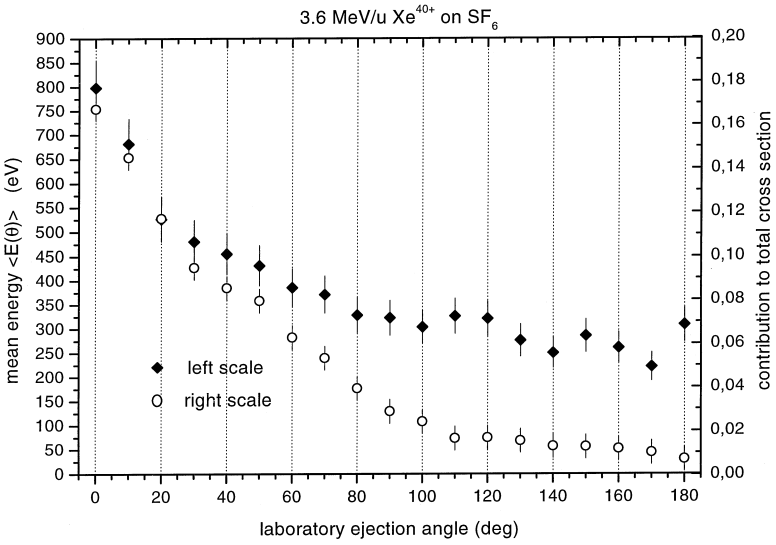

Fig. 4. Right scale: Contribution of a section 10° wide at angle ϑ to the total emission in collisions of 3.6 MeV/u Xe^{40+} with SF_6. Left scale: Mean electron emission energies.

3.4. Mean ejected electron energy in collisions with 5.9 MeV/u U^{29+}

Dramatic changes in the momentum plots are observed for the 5.9 MeV/u U^{29+} on octafluorpropane C_3F_8 as it is shown in the spectrum in Fig. 5.

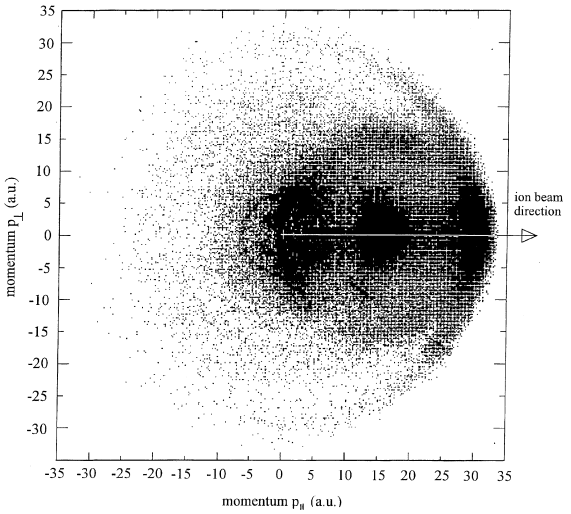

Fig. 5. Complete two-dimensional final state momentum space for electrons emitted in collisions of 5.9 MeV/u U^{29+} with C_3F_8.

The emission at the projectile velocity of 15 a.u. is caused by loosely bound projectile electrons that scatter off the target nucleus, the so-called Electron-Loss-to-the-Continuum peak. Compared to the xenon collision system, the Binary Encounter peak at $2v_P$ is even more pronounced at small emission angles. Furthermore, fast BE electrons that are scattered again off the target nucleus, are visible at $2v_P$ at angles up to 135° [27] (see Fig. 6).

The mean ejected electron energy is as high as 4200 eV at 0°, decreasing to 600 eV at 180°. The mean energy of the electron emission integrated over all ejection angles is 3050 eV, close to the cusp energy of 3260 eV. The ionic charge of the U projectile of 29+ is smaller than the one of the Xe projectile, thus, the post collision interactions of the electrons with the ionic charge is weaker and cannot be responsible for the strong increase in the mean energy. The impact energy is larger, but only by a factor of 1.6. This is not sufficient to explain the large differences of the mean energies. Clearly, the strong increase in electron energy must be attributed to huge enhancement in the production of

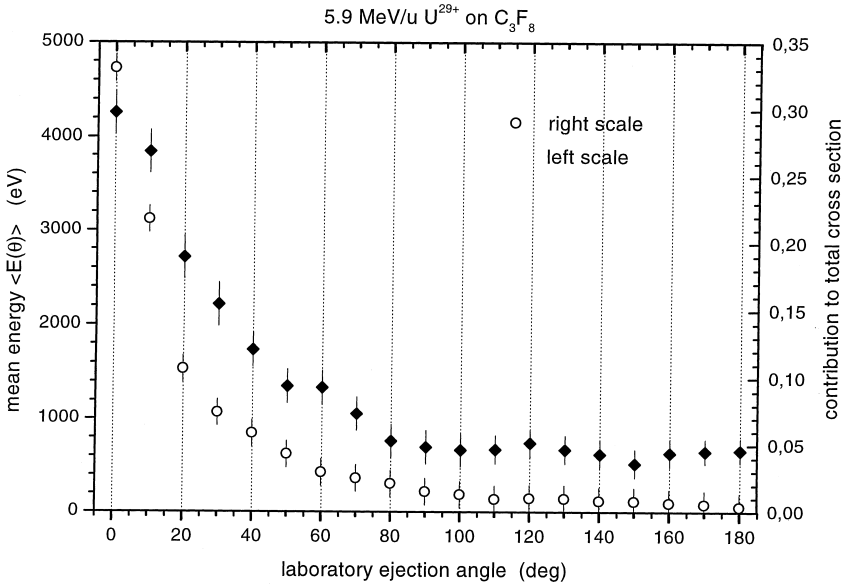

Fig. 6. Right scale: Contribution of a section 10° wide at angle ϑ to the total emission in collisions of 5.88 MeV/u U^{29+} with C_3F_8. Left scale: Mean electron emission energies.

BE electrons in the forward direction. Compared to a scaling with q^2 the enhancement at 0° is 50. Moreover, there is the strong contribution of projectile electrons, that are scattered off the target potential at 3260 eV. At forward angles (−5 to 5°) 25% of all electrons originate from this process. In the transition from bare to highly screened ions it is obvious, that the mean energy of the emitted electrons increases dramatically. In collisions with the U^{29+} a jet of hot electrons is formed, containing two-thirds of the total emission cross section in a cone with 25° opening angle. In comparison to the Ne collision system, the mean electron energy is larger by a factor of 9.

A summary of the last three sections is presented in Table 1. The first column indicates the projectile species, the second the mean ejection energy in the angular range of −25 to 25° around the beam direction and the third the contribution of this section to the total spectrum.

The table shows clearly, that the emission distribution narrows down and is focused in the direction of the projectile trajectory, while the energy increases rapidly. Only to a certain amount the increase can be attributed to interactions of 'slow' outgoing electrons after the collision that are accelerated towards the forward direction in the field of the receding projectile. However, more important for the mean energy is the amount of electrons that originate in ELC and BE processes in the field of a highly screened projectile. This might explain the differences of the mean energies measured in our experiment to those measured by Schneider et al. [28] and Jung et al. [29], where collisions of highly charged ions on thin carbon foils were examined. In these references mean energies of electron emission are lower than in this paper. For the 8 MeV/u U^{68+} on carbon foil collision system Schneider et al. obtain a value of $\langle E \rangle = 880$ eV in forward direction. We attribute this difference to the higher charge state of the uranium projectile, that is in fact, close to equilibrium. As pointed out in [19] the enhancement of BE electron production is most prominent for energies around 6 MeV/u and low charge states. Furthermore, there are more electrons at 3200 eV from the Electron-Loss process. A third source of the discrepancy is the reduced detection efficiency for low energy electrons (10–200 eV) in our data, but as already stated, we estimate this error not to be larger than 10–15%.

Table 1
Mean electron ejection energies and percentage of the total emission cross section for 3.6 MeV/u Ne^{10+}, Xe^{40+} and 5.9 MeV/u U^{29+}

Projectile	$\langle E_e$ (−25 to 25°) $\rangle$ (eV)	% of total cross section (%)
Ne	505	29.3
Xe	686	43.7
U	3912	66.0

In order to discuss the effects of target structure on the mean ejected electron energies, the dependence on the number of target electrons is given in Fig. 7.

The mean energy of electrons is basically constant over the range of electron numbers (10–90). There is an increase in mean energies for the

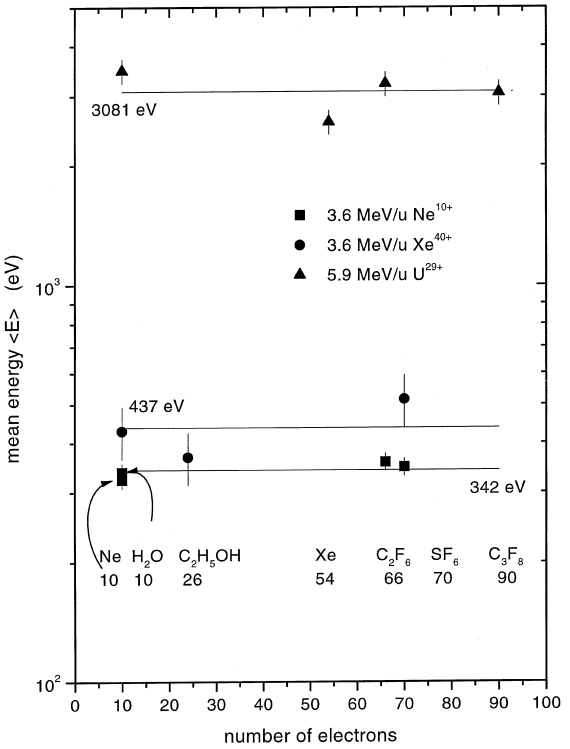

Fig. 7. Mean energies of all measured projectiles and targets.

nuclear charge of the projectile, but not for its charge state q, indicating, that only the effects due to projectile screening play a role for the energy of the ejected electrons. Within the errors only the mean electron energy for uranium on xenon is slightly shifted to below average. This might be explained by the high Z of the xenon target, resulting in the highest net binding energy that has to be brought up for ionization.

4. Impact parameter dependent electron emission

4.1. The nCTMC-calculations

A many-body classical trajectory Monte Carlo (*n*CTMC) code developed by Olson and Salop [30] was used to calculate double differential cross sections of electron production and impact parameter dependencies of capture processes, recoil ion charge distributions and mean electron energies. Within the framework of these classical calculations quantum–mechanical aspects like interferences and selection rules are neglected. Despite of this, the *n*CTMC method has been proven to be successful in the prediction of cross sections and transition probabilities, especially in many-body problems, that cannot be treated analytically.

In an atom modeled by the *n*CTMC, the momentum distribution for a Coulomb potential is identical with the quantum–mechanical approach, but the spatial distribution is not. The actual collision process is calculated by solving the classical Hamiltonian for each of the particles. The calculation is stopped, when the projectile distance is larger than 30 a.u. to the target atom. Then for each electron is checked whether its kinetic energy is either less than the target potential at this place (no ionization), or less than the projectile potential at this place (capture), or more than either of the potentials (free, ionized electron).

The calculations for the neon projectile were carried out using a pure Coulomb ($1/r$) potential, whereas for the xenon projectile a Green–Garvey model potential with $q=40$ and a screening term was employed [31].

Fig. 8 shows the capture probability for the neon and xenon projectiles in dependence of the impact parameter. For the neon projectile 170.000 trajectories were calculated where ≈13.000 captures occurred. For the xenon we evaluated 60 000 trajectories with 29 700 events.

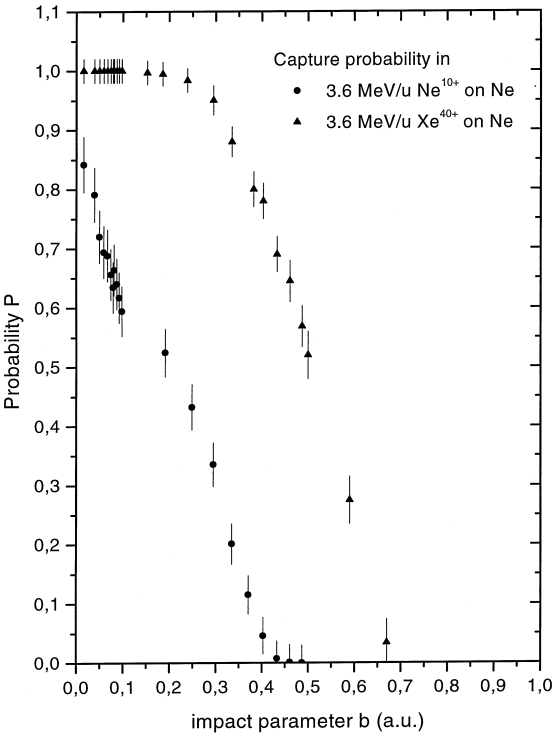

Fig. 8. Calculated probability of a capture event in dependence on the impact parameter for isotachic bare neon (dots) and Xe^{40+} (triangles).

We define the capture radius r_c as the maximum impact parameter if 95% of all capture events take place within its limits. The figure shows that r_c is about 0.35 a.u. for Ne^{10+} and 0.65 a.u. for Xe^{40+} projectiles. This is somewhat lower than half the lattice constant for most solid targets, that is in the order of 1–2 a.u. Consequently a coincidence of a capture process and an electron is equivalent to a collision at small impact parameters in the order of the mean distance of neighboring atoms in a solid.

4.2. Coincidence measurements in collisions with 3.6 MeV/u Xe^{40+}

In the upper part of Fig. 9, two spectra are displayed. The first spectrum shows the singly

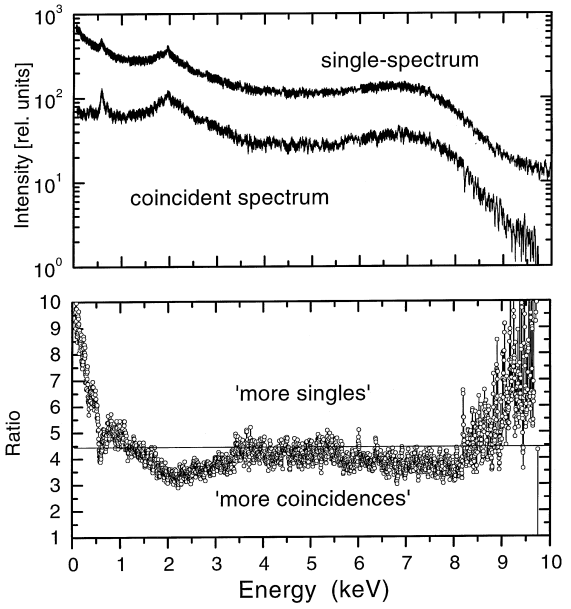

Fig. 9. Top: Single differential energy spectrum (integrated from 0° to 360°) of the collision system 3.6 MeV/u Xe^{40+} on SF_6. The upper spectrum is taken in single mode without coincidences. For the lower spectrum the condition was set on electron capture of the projectile. Bottom: Ratio of single over coincident spectrum.

differential cross section $d\sigma/dE$ of electron emission in the 3.6 MeV/u Xe^{40+} on SF_6 collision system. All ejection angles are integrated in this non-coincident ('singles') spectrum. The cross section is multiplied by the emission energy to enhance visibility of structures at the high energy end of the spectrum. The second spectrum below shows the electron energy distribution when another electron of the target atom has been captured by the projectile and thus a coincidence has occurred. In the lower part of the figure the ratio of both spectra

$$R = \frac{d\sigma/dE_{\text{single}}}{d\sigma/dE_{\text{coincident}}}$$

is presented. The ratio R seems suitable to discuss the differences in the two spectra.

The average ratio $R = 4.1$ is plotted as a reference line to decide whether the electron emission for the coincident spectrum is enhanced or reduced over the singles spectrum. A ratio larger than 4.1 indicates that there are relatively more electrons than average emitted in the singles spectrum than in the coincident spectrum and vice versa. The ratio shows some minima and maxima in distinct emission energy regions, which are attributed to the following emission processes. In the low energy region up to 1 keV the ratio decreases from 10 to 4. The emission of low energy electrons is suppressed when the capture condition is requested. In collisions with impact parameters smaller than r_c the mean momentum transfer is larger as in collision where all impact parameters are accounted for. The steady decrease in the ratio between 10 and 1000 eV is interrupted by the emission of the F-KLL Auger electrons. In these collisions an inner shell electron of the fluorine atoms has to be ionized, which can only take place, when the impact parameter is about the K-shell radius for fluorine. In the region between 1200 and 3500 eV the ratio tends to be smaller than 4. The probability for the emission of an ECC electron at the beam velocity (≈2000 eV) is enhanced when the condition is set to the capture process. Obviously, capture into bound or continuum states of the projectiles takes place at similar impact parameters. In the region from 3500 to 5500 eV the ratio is only slightly smaller than 4.1, thus, the emission of BE electrons at 30–50° ejection angle, that is mainly contributing to the cross section in this energy range, does not depend on the impact parameter. The Binary emission in forward direction from 0° to 30° in the coincident spectrum is again enhanced over the single spectrum: Only hard and close collisions contribute to the production of these electrons, which are more likely, when the projectiles have a trajectory through the electron cloud of the target atom. The strong increase in the ratio beyond 8000 eV is due to background electrons and is not correlated to the capture process. Although R increases to 10, the absolute number of electrons at this energy is very low and does not contribute significantly to the total number of electrons.

As a first result, the condition on a capture results mainly in a decrease of low energy electrons and an enhancement of ECC- and BE-electrons in forward direction. Electrons with intermediate energies do not appear to be significantly affected.

Since the decrease of the relative yield of low energy electrons in the coincidence spectra affects a region with the largest number of electrons, it is the most striking difference between collisions with all impact parameters, or collisions with a b that is limited to 0 to r_c.

4.3. Coincidence measurements in collisions with Ne^{10+}

In less detail, we compare the coincident and single spectra in the 3.6 MeV/u Ne^{10+} on neon collision system, as shown in Fig. 10.

Again, the singly differential cross section (integrated over all angles) is multiplied by E. The singles spectrum without coincidences is dominated by the contribution of low energy electrons. At around 800 eV a strong peak arises from Ne KLL-Auger electrons. The peak at 1970 eV from ECC electrons is neglectable. A distinct Binary peak cannot be seen, because for bare ions there is no enhancement in forward direction and the integration over all angles averages out the peak maxima. For the coincident spectrum the following features can be observed: first, the overall ratio of the two spectra is 25 and the probability for a capture and a second emitted electron is much smaller. On one hand, this is caused by the smaller cross section for electron capture into Ne^{10+}, because it offers less free states with the appropriate energy levels for population than the Xe^{40+}. On the other hand, the probability for multiple ionization in case of the neon projectile is smaller. Second, there is almost no low energy emission, TBE electrons are greatly suppressed and third, the Ne KLL-Auger is the dominant structure in this spectrum and is responsible for almost 50% of the total counts. This leads to the conclusion, that in the close collision selected by the capture process, a K-shell ionization is very likely. This K-hole decays under emission of an Auger electron and leaves the target atom at least in a charge state of 2+. It has been established that the production of an inner shell vacancy by a fast heavy ion is very likely accompanied by 1 or two holes in an outer shell, actually leaving the atom in a charge state $\geqslant 3+$. In a large molecule, the loss of electrons in binding orbitals might lead to a Coulomb explosion. A Coulomb explosion in, for example, a DNA strand is very effective in producing damage to the proliferating capacity of its cell. The K-hole finally results in severe damage of a sensitive target, whereas the ionization of only one electron in the outer shell of the target, although in total

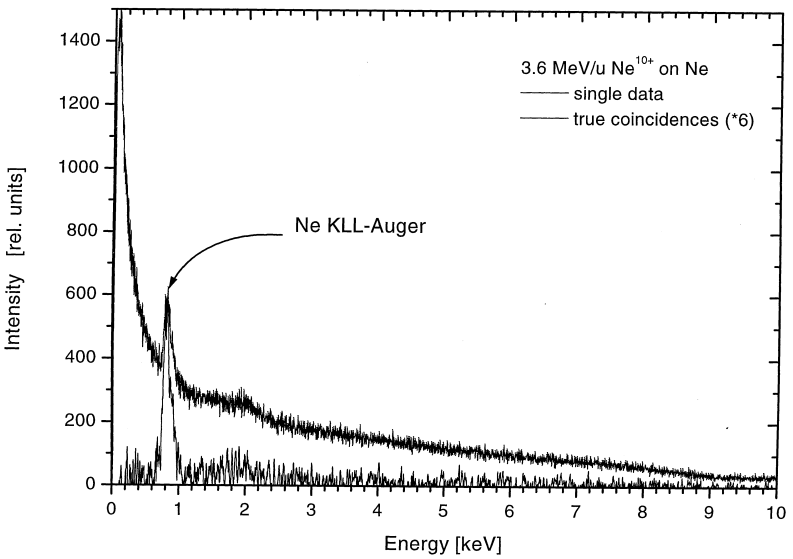

Fig. 10. Same as top of Fig. 9 for the 3.6 MeV/u Ne^{10+} on Ne collision system.

certainly more frequent, is not expressed in damage. In fact, Chetioui et al. [32] proposed a model, where K-shell ionization cross sections by heavy ions were used to explain deactivation cross sections of living cells after heavy-ion radiation. However, it is premature to draw any such far-reaching conclusions from the data shown in this paper.

5. Conclusions

A dramatic increase in the mean energy of the emitted electrons has been found in the transition of collisions of bare to highly screened heavy-ions with many-electron targets. For the bare neon ion, about 30% of the electrons are emitted in a cone with 25° opening half-angle, for the uranium two-thirds of the total cross section are emitted in this angular section. The results for the spectra measured in coincidence with a capture of one electron in the projectile yielded a relative suppression of low energies and an enhancement of the production cross section for high energy electrons. For collisions in a solid state target the consequence of the shift towards higher mean energies is a decrease of deposited dose close to the track of the ion and and an increase in dose in regions far away from the initial primary ionization events. The presented data exhibit evidence for an increased area (widening of the track) of enhanced ionization density along the ion's path through the solid. Although the angular emission characteristics of the secondary electron will be washed out by the many subsequent elastic and inelastic scattering events, the existence of a hot and dense plasma channel along the heavy ion track in the solid is highly probable and deserves further investigation. For the uranium projectile, the initial charge state was well below equilibrium; in a series of collisions with the atoms in a solid, at 5.9 MeV/u it will rapidly increase from 29+ to about 60+, resulting in a less screened ionic potential and, thus, less influence of the described effects. Nevertheless, as it was seen for the xenon projectile the effects are less dramatic for heavy projectiles around equilibrium, but still strong enough to play a decisive role in electron production.

Acknowledgements

The authors are grateful to BMBF (Bonn), DFG (Bonn), GSI Darmstadt and European Community in Brussels for support. SH acknowledges support by the Division of Chemical Sciences, Office of Basic Energy Sciences, Office of Energy Research, US Department of Energy.

References

[1] K.-O. Groeneveld, E. Schopper, S. Schumann, in: H. Francois et al. (Eds.), Solid State Nuclear Track Detectors, Oxford and New York, 1980, pp. 81.
[2] G.W. Barendsen, T.L.J. Beusker, A.J. Vergroesen, L. Budke, Rad. Res. 13 (1960) 841.
[3] F. Bloch, Ann. Phys. 6 (1933) 285.
[4] G. Kraft, M. Krämer, Adv. Rad. Biol. 17 (1993) 1.
[5] G. Kraft, Strahlenther. Onkol. 166 (1990) 10.
[6] M. Krämer, G. Kraft, Rad. Eff. Def. Sol. 126 (1993) 49.
[7] M.E. Rudd, T. Jorgensen , Phys. Rev. 131 (1963) 666.
[8] N. Stolterfoht, Phys. Rep. 146 (1987) 315.
[9] A. Salin, J. Phys. 2 (1969) 631; 5 (1972) 979.
[10] G.B. Crooks, M.E. Rudd, Phys. Rev. Lett. 25 (1970) 1599.
[11] M.E. Rudd, C.A. Sauter, C.L. Bailey, Phys. Rev. 151 (1966) 20.
[12] T.F.M. Bonsen, L. Vriens, Physica 47 (1970) 307.
[13] H. Rothard, Scan. Micr. 9 (1995) 1.
[14] M.E. Rudd, Y.-K. Kim, D.H. Madison, T.J. Gay, Rev. Mod. Phys. 64 (1992) 441.
[15] L.H. Toburen, Scan. Micr. Supp. 4 (1990) 239.
[16] U. Ramm, U. Bechthold, O. Jagutzki, S. Hagmann, G. Kraft, H. Schmidt-Böcking, Nucl. Inst. and Meth. B 98 (1995) 359.
[17] C. Kelbch, R.E. Olson, S. Schmidt, H. Schmidt-Böcking, J. Phys. B 22 (1989) 2171.
[18] R.E. Olson, C.O. Reinhold, D.R. Schultz, J. Phys. B 23 (1990) L455.
[19] D.R. Schultz, R.E. Olson, J. Phys. B 24 (1991) 3409.
[20] C.P. Bhalla, R. Shingal, J. Phys. B 24 (1991) 3187.
[21] C. Reinhold, D.R. Schultz, ,R.E. Olsen .J.Phys. B 23 (1990) L591.
[22] S. Hagmann et al., J. Phys. B 25 (1992) L287.
[23] W. Wolff et al., J. Phys B 25 (1992) 3683.
[24] M. Laßmann, H. Roos, A.M. Kellerer, Rad. Prot. Dos. 52 (1994) 51.
[25] P. Richard, D.H. Lee, T.J.M. Zouros, J.M. Sanders, J.L. Shinpaugh, J. Phys. B 23 (1990) L213.
[26] U. Bechthold, S. Hagmann, J. Ullrich, U. Ramm, G. Kraft, D.R. Schultz, C.O. Reinhold, H. Schmidt-Böcking, accepted by Phys. Rev. A.
[27] U. Bechthold, S. Hagmann, J. Ullrich, B. Bathelt, A. Bohris, R. Moshammer, U. Ramm, C. Bhalla, G. Kraft, H. Schmidt-Böcking, Phys. Rev. Lett. 79 (1997) 2034.

[28] D. Schneider, G. Schiwietz, D. DeWitt, Phys. Rev. A 47 (1993) 3945.
[29] M. Jung, H. Rothard, B. Gervais, J. Grandin, A. Clouvas, R. Wünsch, Phys. Rev. A 54 (1996) 4153.
[30] R.E. Olson, A. Salop, Phys. Rev A 16 (1997) 531.
[31] A.E.S. Green, D.L. Sellin, A.S. Zachor, Phys. Rev 184 (1969) 1.
[32] A. Chetioui, I. Despiney, L. Guiraud, L. Adoui, L. Sabatier, B. Dutrillaux, Int. J. Radiat. Biol 65 (1994) 511.
[33] D.H. Lee, P. Richard, T.J.M. Zouros, J.M. Sanders, J.L. Shinpaugh, H. Hidmi, Phys. Rev. A 41 (1990) 4816.